Structure-property coupling in $Sr_{3}(Ru_{1-x}Mn_{x})_{2}O_{7}$

Biao Hu, Gregory T. McCandless, V. O. Garlea, S. Stadler, Yimin Xiong, Julia Y. Chan, E. W. Plummer, and R. Jin

Phys. Rev. B **84**, 174411 — Published 11 November 2011

DOI: 10.1103/PhysRevB.84.174411

Structure-Property Coupling in $Sr_3(Ru_{1-x}Mn_x)_2O_7$

Biao Hu[1], Gregory T. McCandless[2], V. O. Garlea[3], S. Stadler[1],
Yimin Xiong[1], Julia Y. Chan[2], E. W. Plummer[1] and R. Jin[1,*]
[1]*Department of Physics & Astronomy, Louisiana State University, Baton Rouge, Louisiana 70803, USA*
[2]*Department of Chemistry, Louisiana State University, Baton Rouge, Louisiana 70803, USA and*
[3]*Neutron Scattering Sciences Division, Oak Ridge National Laboratory, Oak Ridge, Tennessee 37831, USA*

Layered ruthenates are prototype materials for the study of structure-property correlations. We report the structural and physical properties of double-layered perovskite $Sr_3(Ru_{1-x}Mn_x)_2O_7$ single crystals with $0 \leq x \leq 0.7$. Single crystal x-ray diffraction refinements reveal that Mn doping on the Ru site leads to the shrinkage of unit-cell volume and disappearance of $(Ru/Mn)O_6$ octahedron rotation when $x > 0.16$, but the crystal structure remains tetragonal. Upon doping, the electrical resistivity reveals metallic character ($d\rho/dT > 0$) at high temperatures but insulating behavior ($d\rho/dT < 0$) below a characteristic temperature T_{MIT}. Interestingly, T_{MIT} is different from T_M, at which magnetic susceptibility reaches maximum. While T_{MIT} monotonically increases with increasing x, T_M shows non-monotonic dependence with x even though the effective spin increases from $S \sim 1$ (x=0) to $\sim 3/2$ (x=0.7). The phase diagram consists of three distinct magnetic ground states, due to local structure change.

PACS numbers: 74.70.Pq, 71.30.+h, 71.27.+a, 61.05.cp

Transition metal oxides (TMOs) have attracted considerable attention due to the strong correlations between charge, lattice, orbital, and spin degrees of freedom. The Ruddleson-Popper (RP) $Sr_{n+1}Ru_nO_{3n+1}$ (n=integer) series are prototype strongly correlated systems, since both theoretical and experimental investigations indicate intimate relationships between structural, electronic and magnetic properties [1–5]. A change in local structure often results in different ground states, as seen in single-layered (n=1) $Ca_{2-x}Sr_xRuO_4$ [6, 7]. Different from the rest of the RP series, $Sr_3Ru_2O_7$ (n=2) shows unique physical properties. Although the electrical resistivity varies smoothly with temperature without any anomaly, the magnetic susceptibility of $Sr_3Ru_2O_7$ reveals a characteristic peak around 16 K [2]. While density functional calculations predict that $Sr_3Ru_2O_7$ is an itinerant system with ferromagnetic (FM) ordering tendencies [8], neutron scattering measurements confirm that the susceptibility peak corresponds to a short-range antiferromagnetic (AFM) correlation [9, 10]. Under the application of hydrostatic pressure, the ground state of $Sr_3Ru_2O_7$ reveals FM instability [2]. On the other hand, the application of magnetic field leads to a metamagnetic transition at low temperatures [11]. These phenomena strongly suggest that both AFM and FM interactions are inherent in $Sr_3Ru_2O_7$.

It was reported that a small substitution of Ru by Mn drives the ground state from a paramagnetic metal (PM) to an AFM insulator (Mott type), and a phase diagram of $Sr_3(Ru_{1-x}Mn_x)_2O_7$ was mapped out up to x=0.2 [12]. X-ray absorption spectroscopy (XAS) indicated that the Mn dopant has an oxidation state different from Ru^{4+} [13], while x-ray photoemission spectroscopy (XPS) showed no sign of doping-induced multiple Ru valences up to x=0.2 [14]. We have studied $Sr_3(Ru_{1-x}Mn_x)_2O_7$ over an extended doping range with $0 \leq x \leq 0.7$. According to its electronic and magnetic properties, a phase diagram is constructed which has two phase boundaries: one is a metal-insulator crossover line and the other is the magnetic transition line, even though they start off together at low doping levels as reported previously [12]. Through our results, we address the central issue: how Mn doping leads to the change of ground state properties.

Single crystals of $Sr_3(Ru_{1-x}Mn_x)_2O_7$ ($0 \leq x \leq 0.7$) were grown by the floating-zone technique in an image furnace. To avoid oxygen deficiency, 10 atmosphere oxygen pressure is applied during the growth. All selected crystals for physical property measurements shown here were characterized by powder and single crystal x-ray diffraction (XRD). The crystal structure and Mn concentration (x) were determined by single crystal XRD refinement. Magnetic susceptibility measurements were carried out in a SQUID magnetometer. Measurements of the resistivity and specific heat were performed in a PPMS.

For all $Sr_3(Ru_{1-x}Mn_x)_2O_7$ samples, single crystal XRD data show that their structure can be described by the space group $I4/mmm$ with the details described previously [15]. Fig. 1(a) displays the unit-cell representation of $Sr_3(Ru_{1-x}Mn_x)_2O_7$ and Fig. 1(b) illustrates the three oxygen sites of the $(Ru/Mn)O_6$ octahedron. Fig. 1(c) shows the x dependence of lat-

*Electronic address: rjin@lsu.edu

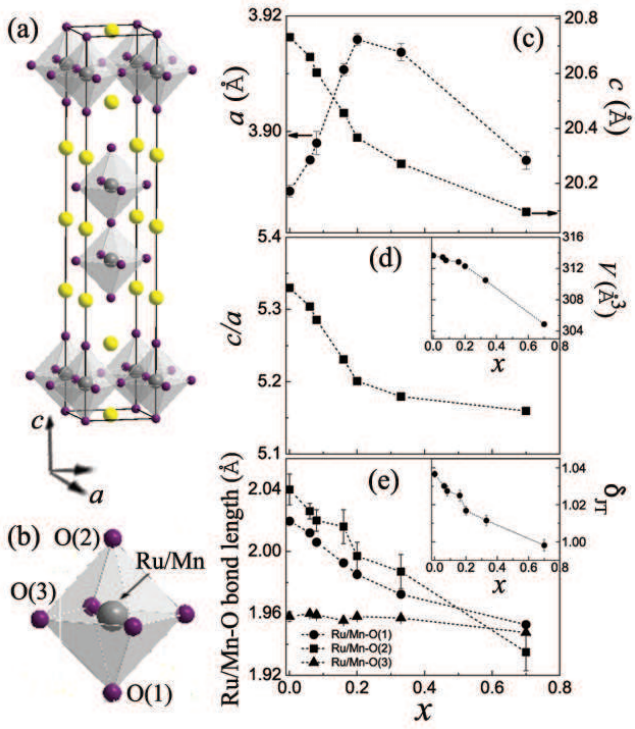

FIG. 1: (Color online) Unit-cell representation of $Sr_3(Ru_{1-x}Mn_x)_2O_7$ in space group $I4/mmm$ (a) and the configuration of the $(Ru/Mn)O_6$ octahedron (b), where the Mn atoms partially occupy the Ru site. (c)-(e) are the x dependence of the lattice parameters a and c, the ratio c/a and the rotation angle ϕ of the $(Ru/Mn)O_6$ octahedron and the bond lengths of Ru/Mn-O(1) (inner apical), Ru/Mn-O(2) (outer apical), and Ru/Mn-O(3) (equatorial) at 298 K. The insets of (c) and (e) are the unit cell volume V and the Jahn-Teller distortion δ_{JT} as a function of x at 298 K, respectively. Dashed lines are guides for the eye.

tice parameters a and c at 298 K. Note that, with increasing x, a increases for $0\leq x\leq 0.2$ and decreases for $x>0.2$, while c decreases monotonically. This results in a monotonic decrease of the unit cell volume V (see the inset of Fig. 1(d)) and c/a with increasing x, as shown in Fig. 1(d). According to Ref. [16] the volume obtained from polycrystalline $Sr_3Mn_2O_7$ (x=1) is even smaller. This suggests that the ionic radius of Mn is smaller than that of Ru. Remarkably, the Ru/Mn-O(3) bond length remains more or less unchanged, while both the Ru/Mn-O(1) and Ru/Mn-O(2) bond lengths [Fig. 1(e)] decrease with increasing x. The Jahn-Teller distortion (δ_{JT}) can be calculated via δ_{JT}=[Ru/Mn-O(1)+Ru/Mn-O(2)]/[2×Ru/Mn-O(3)], which decreases from 1.04 for x=0 to 1.0 for x=0.7 (see the inset of Fig. 1(e)). This indicates that Mn doping makes the $(Ru/Mn)O_6$ octahedron less distorted. Further support can be found from the reduction of rotation angle of the $(Ru/Mn)O_6$ octahedron, as will be discussed later.

The temperature dependence of the in-plane electrical resistivity (ρ_{ab}) of $Sr_3(Ru_{1-x}Mn_x)_2O_7$ is shown in Fig. 2(a). For the undoped compound (x=0), ρ_{ab}(T) is metallic in the measured temperature range. Upon doping, ρ_{ab} is not only enhanced in magnitude but also changes the sign in slope at a characteristic temperature T_{MIT} from positive (metallic) at high temperatures to negative (insulating) at low temperatures. The out-of-plane electrical resistivity (ρ_c) exhibits very similar temperature and x dependence (not shown), but there is a large anisotropy as shown in the inset of Fig. 2(a). This result is consistent with the previous report that a metal-insulator transition (MIT) occurs when introducing the Mn dopant into $Sr_3Ru_2O_7$ [12]. With increasing x, T_{MIT} is quickly pushed to higher temperatures and the transition becomes less pronounced.

However, the magnetic properties of $Sr_3(Ru_{1-x}Mn_x)_2O_7$ reveal a different trend. Fig. 2(b) shows the temperature dependence of the in-plane magnetic susceptibility (χ_{ab}) under zero-field cooling (ZFC) (χ_{ab} measured under the field-cooling condition is very similar). For $0\leq x\leq 0.7$, χ_{ab} always displays a characteristic peak at T_M. For x=0, T_M is about 16 K, in agreement with previous results [2]. With increasing x, T_M initially increases then decreases, with a maximum ($\sim$ 80 K) near $x\sim$0.16. The out-of-plane magnetic susceptibility (χ_c) reveals (not shown) very similar temperature and x dependence as χ_{ab} and has almost identical value at 300 K for $x>$0.16 (see the inset of Fig. 2(a)).

The resistivity and magnetic susceptibility data reveal two characteristic temperatures (T_{MIT} and T_M) in $Sr_3(Ru_{1-x}Mn_x)_2O_7$. The question is whether they correspond to true phase transitions. The specific heat data shown in Fig. 2(c) allow us to determine the nature of T_{MIT} and T_M. In Fig. 2(c), we plot the specific heat as C_p/T vs T, and shift the data for each doping level for clarity. For each x, the value of C_p at T = 2 K is plotted in the inset of Fig. 2(c). For x=0, C_p varies with T smoothly without any anomaly at $T_M\sim$16 K. This indicates that there is no true phase transition in the undoped compound, consistent with neutron scattering measurements [9]. For x=0.06, there is a clear specific heat anomaly at T_M, indicating a true second order phase transition. Since $T_M\sim T_{MIT}$ for x=0.06, it is unclear whether the phase transition originates from magnetic ordering and/or a metal-insulator transition. Specific heat data for higher doping levels can clarify this. Note that, for x=0.16, the specific heat anomaly presents at $T_M\sim$80 K but not at $T_{MIT}\sim$140 K. This indicates that T_M in the region of $0.06\leq x\leq 0.16$ corresponds to a true phase transition, while T_{MIT} represents a crossover temperature from metallic behavior at high temperatures to

insulating character at low temperatures. Recent neutron scattering experiments confirm long-range AFM ordering below T_M for x=0.16 [17].

Theoretically, the entropy removal upon magnetic ordering is expected to be $S_M = R\ln(2S+1) = 1.09R$ for S=1 and $1.39R$ for S=3/2 (R=8.314 J/mol K). We may estimate the actual entropy removal at T_M by subtracting the background by fitting the experimental data outside of the transition region using a polynomial (dashed line in Fig. 2(c)). By integrating $\Delta C_p/T$ in the transition region, we obtain $\Delta S_M \sim 0.077R$ for x=0.06, $0.64R$ for x=0.08, and $0.77R$ for x=0.16. These values are considerably smaller than the expected values, indicating that only a fraction of the spins are ordered. It is also possible that some of entropy has been removed above T_M. Nevertheless, the specific heat anomaly at T_M can no longer be detected when x>0.16 (see the inset of Fig. 2(c)), suggesting that there is no long-range magnetic ordering at high Mn doping levels. As shown in the inset of Fig. 2(c), the low temperature (2 K) specific heat decreases with increasing x, quickly dropping to a very small value as x>0.16. This is most likely due to the reduction of electronic specific heat, because of the insulating ground state when $x \neq 0$. The electronic specific heat becomes negligible at high Mn doping concentrations.

In order to understand why T_M varies with x non-monotically, we analyze χ_{ab} and χ_c at high temperatures. Both χ_{ab}(T) and χ_c(T) can be fitted with a formula $\chi(T) = \chi_0 + \chi_{CW}(T)$ between 175 K and 390 K. Here χ_0 is the temperature independent term and $\chi_{CW}(T) = C/(T-\Theta_{CW})$ is the Curie-Weiss term with Curie constant $C = N_A p_{eff}^2 \mu_B^2/(3k_B)$ and Curie-Weiss temperature Θ_{CW} (p_{eff} is the effective Bohr magneton number, μ_B is the Bohr magneton, and k_B is the Boltzmann constant). Although not shown, the above formula fits our experimental data very well with standard deviation about 0.1%. For all compounds, χ_0 is more or less constant, in the order of 0.5×10^{-3} cm^3/mol. Plotted in Fig. 3 is the x dependence of p_{eff} (main panel) and Θ_{CW} (inset). Note that both Θ_{CW}^{ab} and Θ_{CW}^{c} are negative with similar magnitude and increase with increasing x for $0 \leq x \leq 0.16$. For x>0.2, Θ_{CW}^{ab} is positive but Θ_{CW}^{c} remains negative. The sign change of Θ_{CW}^{ab} is likely caused by the change from AFM to FM interaction in the ab plane, while the dominant magnetic interaction in c direction remains AFM. Indeed, the in-plane magnetization (M_{ab}) vs field (H) plot shows FM character when x>0.16 (see the inset of Fig. 2(b)). The above fitting also shows that $p_{eff}^{ab} \sim p_{eff}^{c}$. Remarkably, both p_{eff}^{ab} and p_{eff}^{c} increase with x and tend to saturate for x>0.16. For x=0, $p_{eff} \sim 2.8$, corresponding to S=1, according to $p_{eff} = g\sqrt{S(S+1)}$ with g=2 for transition metals.

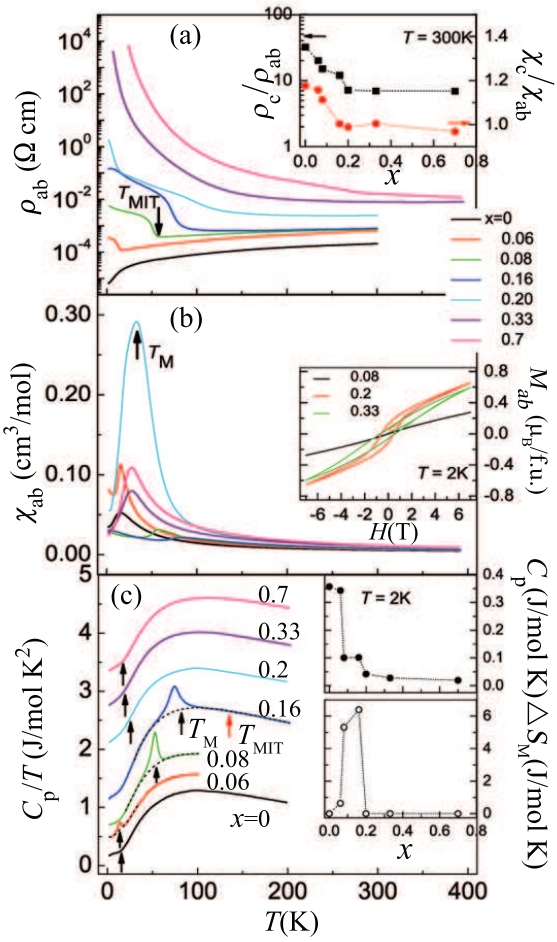

FIG. 2: (Color online) (a) is the temperature dependence of ρ_{ab}(T) with different x. The arrow shows an example of the temperature defined as T_{MIT} for x=0.08. The inset shows the x dependence of ρ_c/ρ_{ab} and χ_c/χ_{ab} at 300 K. (b) is χ_{ab} as a function of T with different x. The arrow shows an example of the temperature defined as T_M for x=0.2. The inset displays in-plane magnetization M_{ab}(H) hysteresis loops at 2 K for x=0.08 (black), 0.2 (red) and 0.33 (green). (c) Temperature dependence of specific heat C_p of $Sr_3(Ru_{1-x}Mn_x)_2O_7$, plotted as $C_p(T)/T$ versus T and shifted for clarity. The black arrows indicate T_M for each concentration. The red arrow indicates T_{MIT} for x=0.16. Dashed lines for each x represent the polynomial fit to the specific heat background. The insets show C_p at 2 K (top) and entropy change at T_M (bottom) for each x.

For x>0.16, $p_{eff} \sim 3.7$, corresponding to S=3/2.

Based on the above observations, we construct a phase diagram for $Sr_3(Ru_{1-x}Mn_x)_2O_7$, covering $0 \leq x \leq 0.7$. Fig. 4 shows the x-T phase diagram, which consists of two boundary lines: T_{MIT} and T_M. In terms of physical properties, it can be divided into five regions, as marked in the phase diagram. Region I represents a paramagnetic (PM) metallic (PM-M) phase, which covers temperature range above T_{MIT}. Region II is a PM insulating (PM-I) phase, where the sys-

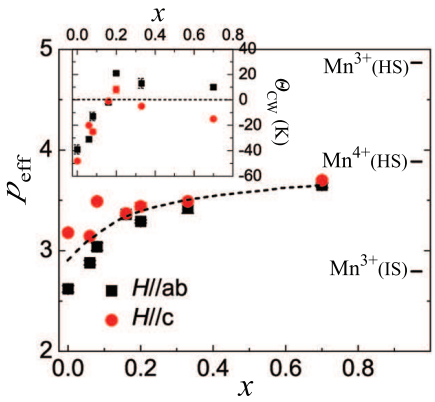

FIG. 3: (Color online) x dependence of the derived $p_{\rm eff}$ from Curie-Weiss law fitting under H$\|$ab and H$\|$c. Dashed lines are guides for the eye. $p_{\rm eff}$ for different Mn oxidation states is also indicated: HS = high spin, IS = intermediate spin. The inset represents the x dependence of the derived $\Theta_{\rm CW}$.

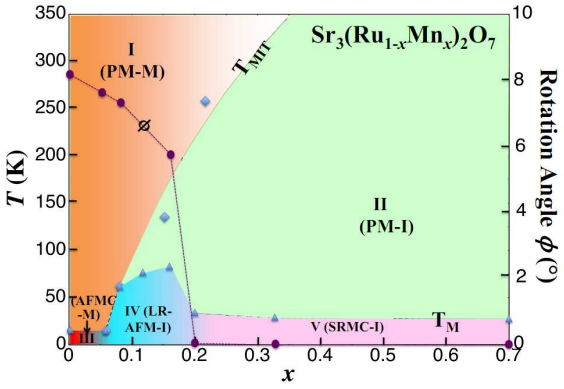

FIG. 4: (Color online) The x-T phase diagram of $Sr_3(Ru_{1-x}Mn_x)_2O_7$ ($0\leq x\leq 0.7$). Diamonds and triangles represent $T_{\rm MIT}$ and $T_{\rm M}$, respectively. Region I is a paramagnetic metallic (PM-M) phase. Region II is a paramagnetic insulating (PM-I) phase. Region III is a metallic phase with AFM correlation (AFMC-M). Region IV represents a long-range AFM insulating phase (LR-AFM-I). Region V is an insulating phase with short-range magnetic correlation (SRMC-I). The right axis shows the x dependence of the rotation angle ϕ of the (Ru/Mn)O_6 octahedron at 90 K.

tem is non-metallic with $d\rho/dT<0$ but remains paramagnetic. Region III ($0\leq x<0.06$) represents metallic phase with AFM correlation (AFMC-M), which is enhanced upon Mn doping. Region IV is a long-range (LR) AFM insulating (LR-AFM-I) phase, where LR AFM ordering forms below $T_{\rm M}$ and the specific heat anomaly emerges at $T_{\rm M}$. Since there is lack of specific heat anomaly, Region V is an insulating phase with short-range magnetic (FM in the ab plane and AFM in the c direction) correlations (SRMC-I). It should be pointed out that there is no conflict between our phase diagram and what presented in Ref [12]. In low doping regime, $T_{\rm MIT}\sim T_{\rm M}$, resulting in single boundary line [12].

In light of all of the structural and physical properties, it becomes clear that the variation of electronic and magnetic properties is intimately connected with the change of local structure of $Sr_3(Ru_{1-x}Mn_x)_2O_7$ even though the global structure symmetry remains unchanged. Due to the partial replacement of Ru by Mn with smaller ionic radius, the unit cell becomes smaller and (Ru/Mn)O_6 becomes less distorted. This is reflected in both rotation angle (see Fig. 4) and Jahn-Teller distortion parameter $\delta_{\rm JT}$ (see the inset of Fig. 1 (e)). This weakens the FM interaction, according to the theoretical calculations for the single layered ruthenate $Ca_{2-x}Sr_xRuO_4$ [5], and leads to long-range AFM ordering in Region IV. When $x>0.16$, (Ru/Mn)O_6 no longer rotates which gives rise to competitive AFM and FM interactions (see the inset of Fig. 3). As a result, the system can no longer form long-range magnetic ordering (Region V). On the other hand, the increase of $T_{\rm MIT}$ with x is not surprising, as $3d$-Mn is more localized than $4d$-Ru.

What is remarkable is that small amount of Mn doping can drive the system into an insulating ground state. In previous studies, optical conductivity spectra reveal evidence for Mott-type metal-insulator transition [12]. This suggests that Mn doping narrows the bandwidth thus enhancing electron-electron correlation. Is band filling also changed? According to XAS data, Mn acts as 3+ in $Sr_3(Ru_{0.9}Mn_{0.1})_2O_7$ [13]. If this were the case, one would expect (1) expansion of the lattice unit cell as Mn^{3+} ($0.65\mathring{A}$) has large ionic radius than Ru^{4+} ($0.62\mathring{A}$), (2) effective $S\sim 2$ for high spin (HS) state or $S=1$ for intermediate spin (IS) state, (3) Ru would exhibit 5+ valence, or (4) oxygen deficiency while Ru remains 4+. Scenarios (1), (2) and (3) may be ruled out, since (1) our XRD data reveal the shrinkage of the unit cell (Fig. 1(c)), (2) high-temperature magnetic susceptibility indicates the increase of S from 1 at $x=0$ to $\sim 3/2$ at $x=0.7$ (Fig. 3), and (3) XPS data exhibit no change in Ru spectra for Mn-doped compounds [14]. On the other hand, scenario (4) is also unlikely as all of our single crystal samples were grown under 10 atmosphere oxygen pressure and our single crystal x-ray refinement provides no evidence for oxygen deficiency. Thus, it is most likely that the oxidation state of Mn in $Sr_3(Ru_{1-x}Mn_x)_2O_7$ is 4+, independant of x. Thus, Mn doping in $Sr_3(Ru_{1-x}Mn_x)_2O_7$ is isovalent while band filling remains unchanged.

In summary, we have investigated the structural and physical properties of Mn-doped $Sr_3Ru_2O_7$ and constructed a rich phase diagram for $0\leq x\leq 0.7$. Two

characteristic temperatures (T_{MIT} and T_{M}) are required to accurately describe the change of the physical properties. T_{MIT} shows a monotonic change, while T_{M} reveals a non-monotonic dependence with x. Three distinct regions are identified below T_{M}, which is driven by the local structure change. This work illustrates that isovalent doping is an effective approach for studying correlated effect on physical properties.

Work at LSU was partially supported by US National Science Foundation with Grant Nos. DMR-1002622 (B. H., E. W. P., and R. J.) and DMR-1063735 (J. Y. C.). The work at the High Flux Isotope Reactor, Oak Ridge National Laboratory, was sponsored by the Scientific User Facilities Division, Office of Basic Energy Sciences, U.S. Department of Energy.

[1] Y. Maeno, H. Hashimoto, K. Yoshida, S. Nishizaki, T. Fujita, J. G. Bednorz, and F. Lichtenberg, Nature (London) **372**, 532 (1994).

[2] S. I. Ikeda, Y. Maeno, S. Nakatsuji, M. Kosaka, and Y. Uwatoko, Phys. Rev. B **62**, R6089 (2000).

[3] D. Fobes, M. H. Yu, M. Zhou, J. Hooper, C. J. O'Connor, M. Rosario, and Z. Q. Mao, Phys. Rev. B **75**, 094429 (2007).

[4] G. Cao and P. Schlottmann, Mod. Phys. Lett. **22**, 1785 (2008).

[5] Z. Fang and K. Terakura, Phys. Rev. B **64**, 020509 (2001).

[6] S. Nakatsuji and Y. Maeno, Phys. Rev. Lett. **84**, 2666 (2000).

[7] O. Friedt, M. Braden, G. Andre, P. Adelmann, S. Nakatsuji, and Y. Maeno, Phys. Rev. B **63**, 174432 (2001).

[8] D. J. Singh and I. I. Mazin, Phys. Rev. B **63**, 165101 (2001).

[9] L. Capogna, E. M. Forgan, S. M. Hayden, A. Wildes, J. A. Duffy, A. P. Mackenzie, R. S. Perry, S. Ikeda, Y. Maeno, and S. P. Brown, Phys. Rev. B **67**, 012504 (2003).

[10] M. B. Stone, M. D. Lumsden, R. Jin, B. C. Sales, D. Mandrus, and S. E. Nagler, Phys. Rev. B **73**, 174426 (2006).

[11] R. S. Perry, L. M. Galvin, S. A. Grigera, L. Capogna, A. J. Schofield, A. P. Mackenzie, M. Chiao, S. R. Julian, S. I. Ikeda, S. Nakatsuji, Y. Maeno, and C. Pfleiderer, Phys. Rev. Lett. **86**, 2661 (2001).

[12] R. Mathieu, A. Asamitsu, Y. Kaneko, J. P. He, X. Z. Yu, R. Kumai, Y. Onose, N. Takeshia, T. Arima, H. Takagi, and Y. Tokura, Phys. Rev. B **72**, 092404 (2005).

[13] M. A. Hossain, Z. Hu, M. W. Haverkort, T. Burnus, C. F. Chang, S. Klein, J. D. Denlinger, H.-J. Lin, C. T. Chen, R. Mathieu, Y. Kaneko, Y. Tokura, S. Satow, Y. Yoshida, H. Takagi, A. Tanaka, I. S. Elfimov, G. A. Sawatzky, L. H. Tjeng, and A. Damascelli, Phys. Rev. Lett. **101**, 016404 (2008).

[14] H. Guo, Yi Li, Darwin Urbina, Biao Hu, Rongying Jin, Tijiang Liu, David Fobes, Zhiqiang Mao, E. W. Plummer, and Jiandi Zhang, Phys. Rev. B **81**, 155121 (2010).

[15] B. Hu, Gregory T. McCandless, Melissa Menard, V. B. Nascimento, Julia Y. Chan, E. W. Plummer, and R. Jin, Phys. Rev. B **81**, 184104 (2010).

[16] J. F. Mitchell, J. E. Millburn, M. Medarde, S. Short, J. D. Jorgensen, and M. T. Fernandez-Diaz, J. Solid State Chem. **141**, 599 (1998).

[17] D. Mesa, F. Ye, S. Chi, J. Fernandez-Baca, B. Hu, R. Jin, E. W. Plummer, and Jiandi Zhang, Unpublished